

# Cumulative Deformation Capacity of Steel Braces under Various Cyclic Loading Histories

Toru Takeuchi, A.M.ASCE<sup>1</sup>; and Ryota Matsui<sup>2</sup>

**Abstract:** The postbuckling behavior of seismic-resistant braces in steel frames under a cyclic axial force is often evaluated by time–history analyses; however, brace fracture is seldom considered. The authors previously proposed a physical model for predicting the moment of fracture of circular-tube braces after buckling using phenomenological hysteresis. However, the accuracy of that model was confirmed only against the test results of the gradually increasing amplitude loading protocol, and its applicability under other loading histories has not yet been verified. In this study, cyclic loading tests were carried out until fracture on circular-tube and H-section braces under various loading histories, followed by FEM analyses. The validity of the proposed formulas for evaluating the strain-concentration index under various loading histories was examined. The proposed method was used for predicting the moment of fracture and the cumulative deformation capacity until fracture, and the predictions agreed well with the test results. DOI: 10.1061/(ASCE)ST.1943-541X.0001146. This work is made available under the terms of the Creative Commons Attribution 4.0 International license, <http://creativecommons.org/licenses/by/4.0/>.

**Author keywords:** Circular hollow section brace; H-section brace; Local buckling; Loading history; Cumulative deformation capacity; Fracture; Seismic effects.

## Introduction

Circular-tube or H-section members are commonly used in seismic-resistant axial elements such as truss structures or diagonal braces in concentrically braced frames (CBFs), together with rectangular hollow sections. When a seismic force exceeds the buckling strength, these brace sections are subjected to cyclic loading after buckling. Various hysteresis curve models have been proposed for such braces (e.g., Prathuangsit et al. 1978; Jain et al. 1978; Popov et al. 1979; Shibata 1982) and are commonly used for performing time–history response analyses of braced structures, including postbuckling behavior. However, these braces are subjected to local buckling near their midpoint, which results in fracture soon after; such fractures are not considered in ordinary time–history analyses. The results of Jain et al. (1980), Tremblay (2002), and Elchalakani et al. (2003) indicate that the fatigue performance of hollow-section members depends on the diameter-to-thickness and slenderness ratios, and that local buckling degrades cumulative deformation capacity. Tang and Goel (1989) proposed formulas for evaluating the cumulative deformation capacity based on these parameters. However, their experimental results showed that the deformation amplitude of the braces is correlated with their performance, thus indicating that the cumulative deformation capacity–strain amplitude relationship is not yet fully understood. Based on their experience with detailed finite-element method analyses, Uriz and Mahin (2004), Kanvinde and Deierlein (2007), Tremblay

(2008), and Fell et al. (2009) proposed a micromechanics-based fracture model of large-scale structural components for explaining the test results. However, such analyses using micro models are time consuming and impractical for general use, especially for large CBFs with many braces, as described by Li et al. (2013). To satisfy such a demand, Hsiao et al. (2013) evaluated the fracture life equations using line-element models against over 40 test results for rectangular hollow-section braces. Takeuchi et al. (2008), and Takeuchi and Matsui (2011) proposed a method that evaluates the cumulative deformation capacity of circular-tube and H-section braces until fracture using phenomenological macro models as the Shibata–Wakabayashi model (Fig. 1, Appendix). In this approach, the local plastic strain estimated using strain concentration ratio formulas are compared to the low-cycle fatigue curves of the material. They validated their method through cyclic loading tests on braces of various sizes. However, the method has only been confirmed using the test results of gradually increasing amplitude loading history, and its applicability under other loading histories has not yet been verified.

In this study, a fracture-prediction method based on the concept of using the strain-concentration ratio index is presented for circular-tube and H-sections, and cyclic loading tests were carried out on said sections under various loading histories until fracture occurred. The buckling hysteresis obtained from the experiments was reproduced using FEM analysis, and the relationship between the local strain in the strain-concentration zone and the normalized axial deformation was investigated for validating the assumptions of the proposed formulas. Finally, the cumulative deformation capacities until fracture of the braces were compared with the corresponding results obtained using the proposed formulas under various loading histories.

## Fracture-Prediction Formulas for Circular-Tube and H-Section Braces

The authors (Takeuchi and Matsui 2011) previously proposed formulas for evaluating the local strain  $\varepsilon_h$  of circular-tube

<sup>1</sup>Professor, Dept. of Architecture and Building Engineering, Tokyo Institute of Technology, M1-29, 2-12-1 O-okayama, Meguro-ku, Tokyo 152-8552, Japan (corresponding author). E-mail: ttoru@arch.titech.ac.jp

<sup>2</sup>Assistant Professor, Dept. of Architecture and Building Engineering, Tokyo Institute of Technology, M1-29, 2-12-1 O-okayama, Meguro-ku, Tokyo 152-8552, Japan.

Note. This manuscript was submitted on November 18, 2013; approved on June 18, 2014; published online on August 14, 2014. Discussion period open until January 14, 2015; separate discussions must be submitted for individual papers. This paper is part of the *Journal of Structural Engineering*, © ASCE, ISSN 0733-9445/04014175(11)/\$25.00.

braces after overall buckling and local buckling as a ratio against normalized axial deformation amplitude  $\Delta\varepsilon_n = \Delta\delta/L$ . Here,  $\delta$  denotes the axial deformation of braces,  $\Delta\delta$  denotes the amplitude of  $\delta$ , and  $L$  denotes the brace length.

$$\alpha_c = \frac{\Delta\varepsilon_h}{\Delta\varepsilon_n} = \begin{cases} 1.0 & (\Delta\varepsilon_n \leq \varepsilon_{cr}, \text{ prebuckling stage and tensile stage}) \\ \frac{\theta_h D}{L_k(1 - \frac{\pi}{4})\Delta\varepsilon_n} & (\varepsilon_{cr} < \Delta\varepsilon_n \leq \varepsilon_{lb}, \text{ overall buckling stage}) \\ \frac{3\sqrt{6}\varphi_h}{\pi\sqrt{\frac{D}{t}}\Delta\varepsilon_n} + \frac{\theta_{lb} D}{L_k(1 - \frac{\pi}{4})\Delta\varepsilon_n} & (\varepsilon_{lb} < \Delta\varepsilon_n, \text{ local buckling stage}) \end{cases} \quad (1)$$

where  $\Delta\varepsilon_h$  = local strain amplitude;  $\theta_h$  = hinge angle;  $D$  = circular tube diameter;  $L_k$  = effective buckling length;  $\varphi_h$  = angle of the skin plate in the local buckling zone;  $\theta_{lb}$  = hinge angle attained at local buckling;  $\varepsilon_{cr} = \sigma_{cr}/E$  = equivalent strain corresponding to overall buckling;  $\sigma_{cr}$  = overall buckling stress; and  $E$  = elastic modulus. By employing Eq. (1), the local strain amplitude,  $\Delta\varepsilon_h$ , in the plastic hinge zone can be calculated by multiplying  $\alpha_c$  and the normalized axial deformation amplitude  $\Delta\varepsilon_n$ . The moment of fracture can be predicted to be the point at which the cumulative local strain amplitude satisfies the low-cycle fatigue criterion of the steel material. These formulas are derived from the simple buckling models shown in Figs. 2 and 3. The effective buckling length,  $L_k$ , is defined in Fig. 4 based on the three-hinge mechanism. In the figure,  $M_{pg}$  denotes the plastic bending moment strength at the connections, and  $M_{pb}$  denotes the plastic bending moment strength at the brace section.

Similar to the procedure for circular-tube braces, the local strain formulas of H-section braces are determined as follows. During overall buckling, a plastic hinge is assumed to occupy the center of the brace, as shown in Fig. 2. The plastic-hinge zone length is calculated using Eq. (2)

$$L_h = L_k \left(1 - \frac{S}{Z}\right) \quad (2)$$

where  $S$  = sectional modulus of the brace about the weak axis and  $Z$  = plastic sectional modulus about the weak axis. The hinge angle,  $\theta_h$ , is expressed by Eq. (3), and the equivalent strain amplitude of the braces on the compression side is determined using Eq. (4), which includes a term for the maximum equivalent tensile strain,  $\varepsilon_{ntm}$ , observed before compression

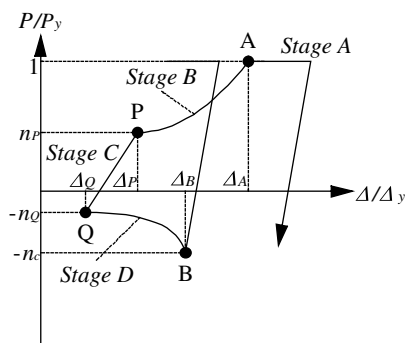


Fig. 1. Shibata-Wakabayashi model for postbuckling hysteresis

The strain concentration ratio  $\alpha_c$  is expressed as a function of  $\Delta\varepsilon_n$  separated into three stages, as given by in Eq. (1): prebuckling and tensile, after overall buckling, and after local buckling

$$\theta_h = \cos^{-1}(1 - \Delta\varepsilon_n) \quad (3)$$

$$\Delta\varepsilon_n = \varepsilon_{ntm} - \varepsilon_n \quad (4)$$

The local strain in the plastic strain concentration zone,  $\varepsilon_h$ , is calculated as the average approximation expressed by Eq. (5)

$$\varepsilon_h = \frac{\theta_h B}{L_h} = \frac{\theta_h B}{L(1 - \frac{S}{Z})} \quad (5)$$

where  $B$  = width of the H-section. The local deformation of the H-section brace during the local buckling stage is modeled as shown in Fig. 5. Eq. (6) expresses the normalized axial deformation that provokes local buckling,  $\varepsilon_{lb}$  (Kato and Nakao 1994), and the hinge angle that leads to local buckling can be calculated using Eq. (7), which is identical to Eq. (3)

$$\varepsilon_{lb} = \frac{3}{2} \left(\frac{2t_f}{B}\right)^2 \quad (6)$$

$$\theta_{lb} = \cos^{-1}(1 - \varepsilon_{lb}) \quad (7)$$

The hinge angle increment in the local buckling zone,  $\Delta\theta_h$ , may be calculated using Eq. (8)

$$\Delta\theta_h = \theta_h - \theta_{lb} \quad (\theta_h > \theta_{lb}) \quad (8)$$

The angle of the skin plate in the local buckling zone,  $\varphi_h$ , is calculated according to Eq. (9) using the hinge angle increment,  $\Delta\theta_h$ , at which local buckling occurs, and vertical angle of local buckling wave,  $\phi$ , as shown in Fig. 5; this is based on the relationship between Eqs. (10) and (11) using the classical plate-buckling theory (Timoshenko and Gere 1961)

$$\varphi_h = \cos^{-1} \left[ \frac{B \sin(\phi - \Delta\theta_h)}{l_p \cos \phi} \right] = \cos^{-1} \left[ \frac{\sin(0.685 - \Delta\theta_h)}{0.6334} \right] \quad (9)$$

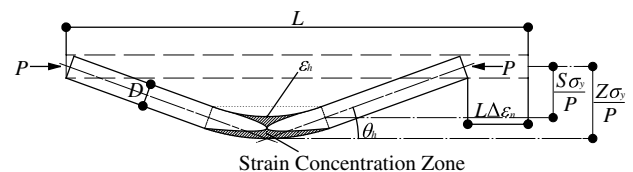


Fig. 2. Plastic hinge model for overall buckling

$$l_p = 1.635 \cdot \frac{B}{2} \quad (10)$$

$$\phi = \tan^{-1} \left( \frac{l_p/B}{2/2} \right) = \tan^{-1}(0.8175) = 0.685 \text{ rad} \quad (11)$$

Here, the bending-moment distribution in the local buckling zone of the flange is assumed as shown Fig. 6, which is the same as that in Fig. 4 for overall buckling. The section of the local buckling area is assumed as rectangular, ratio of the sectional moduli ( $S_l/Z_l$ ) and bending-moment moduli ( $M_y/M_p$ ) becomes

$$\alpha_c = \frac{\Delta \varepsilon_h}{\Delta \varepsilon_n} = \begin{cases} 1.0 & (\Delta \varepsilon_n \leq \varepsilon_{cr}, \text{ prebuckling stage and tensile stage}) \\ \frac{\theta_h D}{L_k \left(1 - \frac{S_l}{Z_l}\right) \Delta \varepsilon_n} & (\varepsilon_{cr} < \Delta \varepsilon_n \leq \varepsilon_{lb}, \text{ overall buckling stage}) \\ \frac{5\varphi_h}{1.635 \left(\frac{B}{2t_f}\right) \Delta \varepsilon_n} + \frac{3}{2\Delta \varepsilon_n} \left(\frac{2t_f}{B}\right)^2 & (\varepsilon_{lb} < \Delta \varepsilon_n, \text{ local buckling stage}) \end{cases} \quad (13)$$

### Cyclic Loading Tests under Various Loading Histories

In previous studies, the results of the proposed Eqs. (1) and (13) were compared with the results of a cyclic-loading test under the gradually increasing amplitude loading history conducted on various circular hollow braces having diameter-to-thickness ratios,  $D/t$ , of 21–32 and slenderness ratios of 50–100, and various H-section braces having width-to-thickness ratios,  $B/2t_f$ , of 6–13 and slenderness ratios of 50–100. The comparison confirmed that the equations could predict the moment of fracture. In this study, cyclic loading tests were carried out under various axial deformation histories. The test setup is shown in Fig. 7, and test specimens' configurations are shown in Fig. 8 and listed in Table 1. The specimens were supported by gusset plates at both ends: one end of a specimen was attached to the reaction frame and the other to the

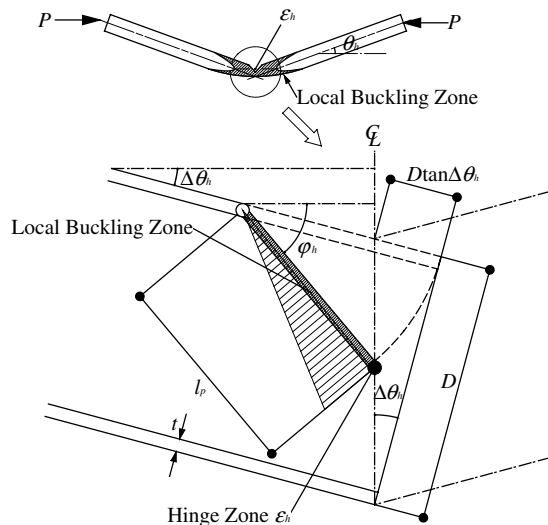


Fig. 3. Local buckling model for circular tubes

sliding table equipped with an actuator. The circular tube braces possessed a slenderness ratio  $\lambda = 70$  and a diameter-to-thickness ratio  $D/t = 28$ , and the H-section braces possessed a slenderness ratio  $\lambda = 70$  and a width-to-thickness ratio  $B/2t_f = 10$ . These ratios were the averages of those of the specimens used in the previous studies.  $L_B$  denotes the distance between the plastic hinges

$$\varepsilon_h = \frac{\varphi_h t_f}{l_{pk} \left(1 - \frac{S_l}{Z_l}\right)} + \varepsilon_{lb} = \frac{5\varphi_h}{1.635 \left(\frac{B}{2t_f}\right)} + \frac{3}{2} \left(\frac{2t_f}{B}\right)^2 \quad (12)$$

Thus, the strain concentration ratio,  $\alpha_c$ , of an H-section is expressed by Eq. (13)

$$\begin{aligned} & (\Delta \varepsilon_n \leq \varepsilon_{cr}, \text{ prebuckling stage and tensile stage}) \\ & (\varepsilon_{cr} < \Delta \varepsilon_n \leq \varepsilon_{lb}, \text{ overall buckling stage}) \\ & (\varepsilon_{lb} < \Delta \varepsilon_n, \text{ local buckling stage}) \end{aligned} \quad (13)$$

sliding table equipped with an actuator. The circular tube braces possessed a slenderness ratio  $\lambda = 70$  and a diameter-to-thickness ratio  $D/t = 28$ , and the H-section braces possessed a slenderness ratio  $\lambda = 70$  and a width-to-thickness ratio  $B/2t_f = 10$ . These ratios were the averages of those of the specimens used in the previous studies.  $L_B$  denotes the distance between the plastic hinges

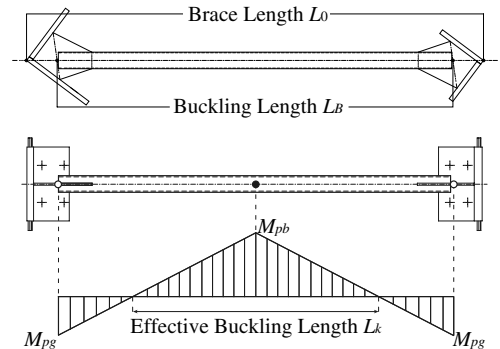


Fig. 4. Effective plastic buckling length

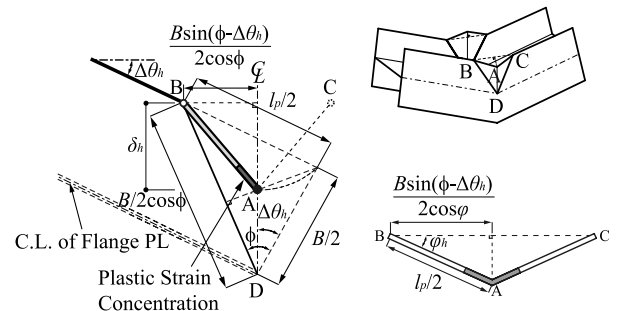


Fig. 5. Local buckling model for H-section

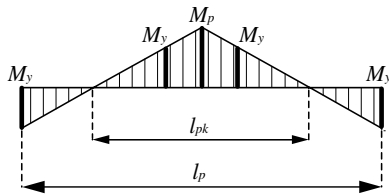


Fig. 6. Effective local buckling length

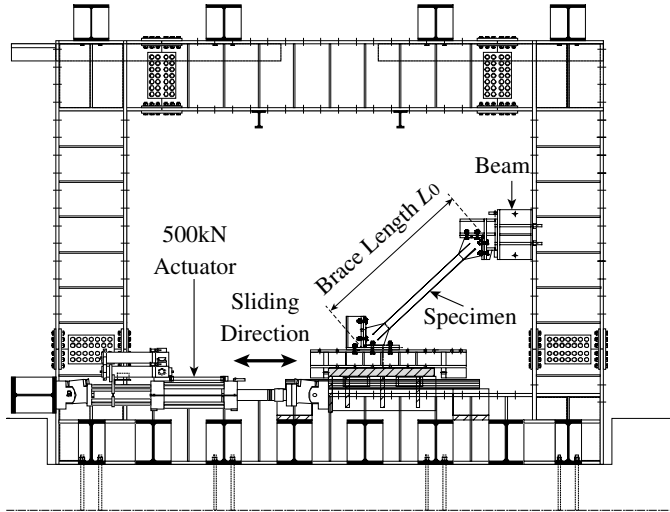


Fig. 7. Test setup

that occurred at both the gusset plates, as shown in Fig. 4. The effective plastic buckling length,  $L_k$ , was estimated to be  $0.76L_B$  for the circular-tube braces and  $0.69L_B$  for the H-section braces. The axial deformation,  $\delta$ , was measured in the test using LVDTs placed between both ends of the base plates. The axial force acting on the specimen,  $P$ , was calculated from the load cell installed in the actuator. The surface strains of the specimens were detected by linear large strain gauges, as shown in Figs. 8(a and b). The normalized axial deformation,  $\varepsilon_n$ , and equivalent stress,  $\sigma_n$ , which are redefined in the following equations, were used as indices

$$\varepsilon_n = \frac{\delta}{L_B}, \quad \sigma_n = \frac{P}{A} \quad (14)$$

where  $A$  = original sectional area of the braces.

In the test, the following axial deformation histories were applied to each specimen. The positive strain indicates tension in the following. When the rigid connection lengths of the quarter of total brace length are assumed in the both sides of 45-degree braces, the normalized axial deformation of the brace meets an approximate value of a story drift ratio.

1. Gradually increasing cyclic amplitude: As shown in Fig. 9(a), the cyclic loading protocol for all of the series was defined by the normalized axial deformation,  $\varepsilon_n$ . The half-amplitude of  $\varepsilon_n$  was increased by 0.1, 0.5, 1.0, and 2.0% for three cycles for each value in the series. After the third cycle at 2.0%, the half-amplitude was maintained at 2.0% until brace fracture.
2. Gradually decreasing cyclic amplitude: As shown in Fig. 9(b), the half-amplitude of  $\varepsilon_n$  was decreased from 1.0% to three cycles each at 0.75% and 0.5%, followed by 0.5% until brace fracture.

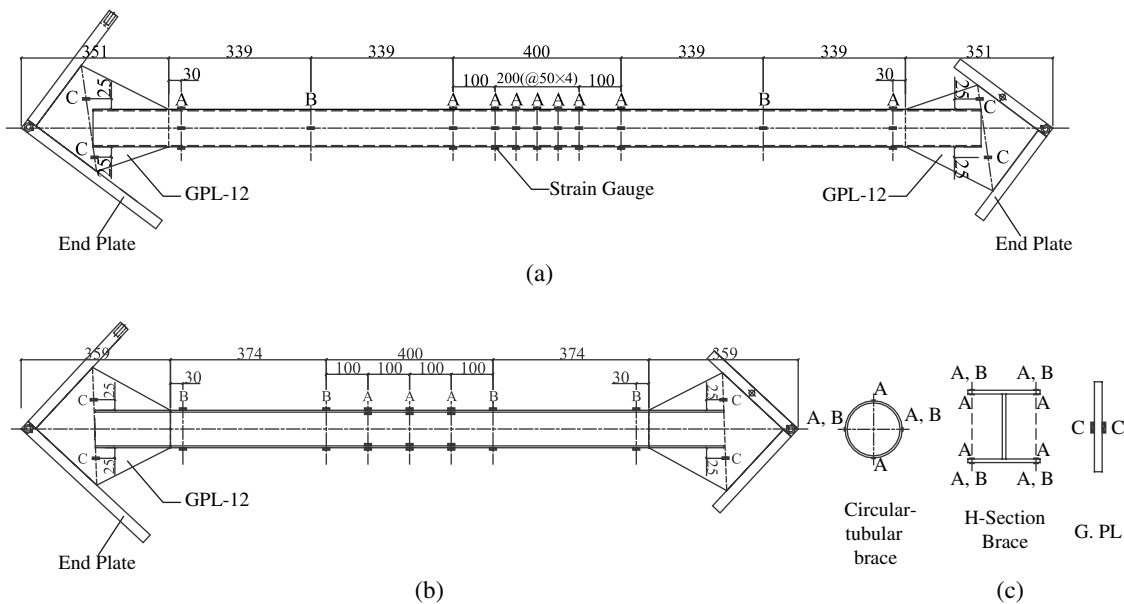
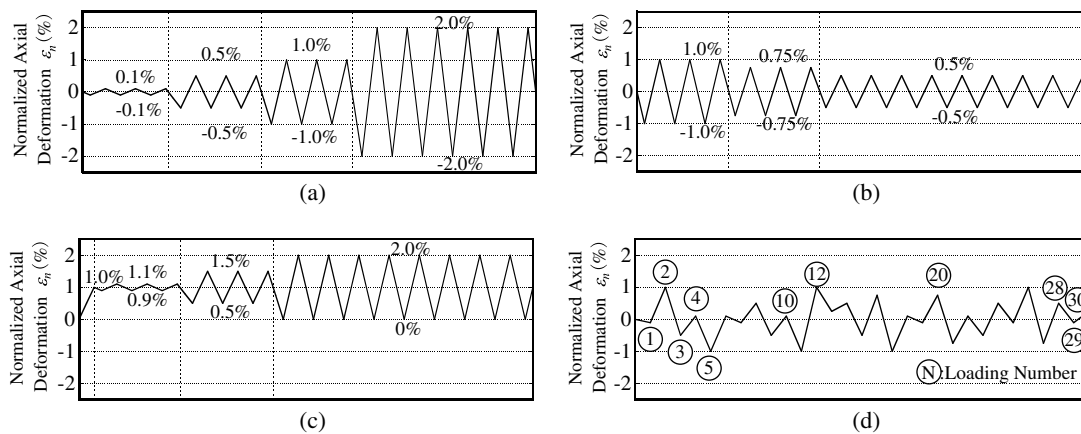


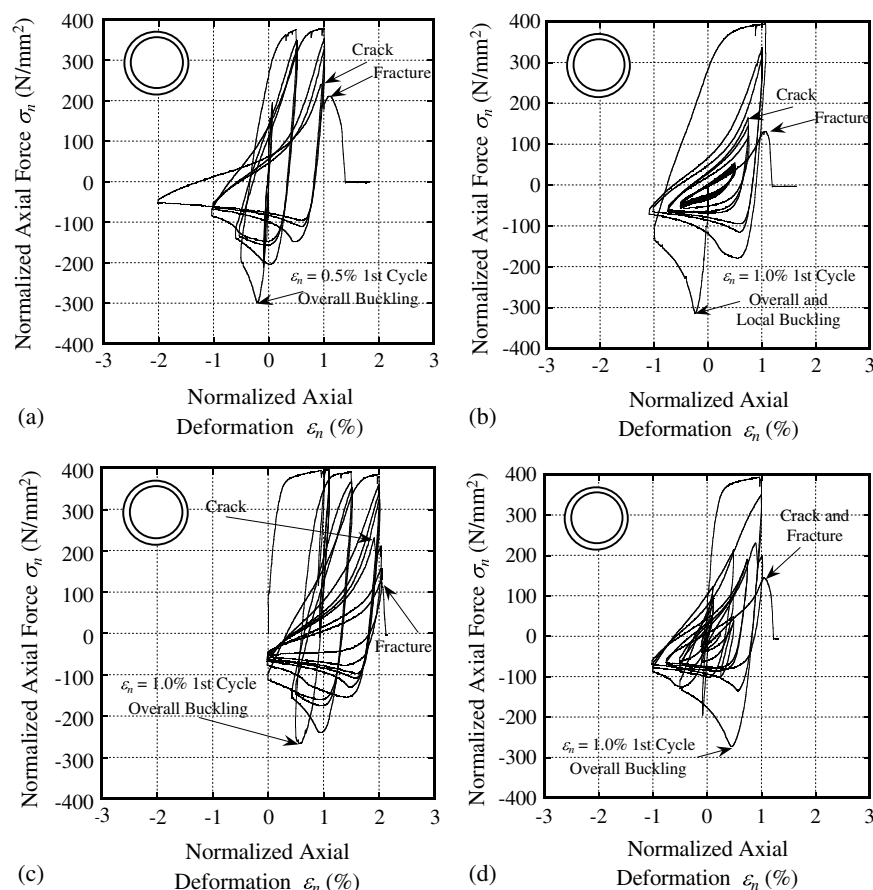
Fig. 8. Test specimen: (a) circular tubular brace; (b) H-section brace; (c) section

Table 1. Specimen Details and Material Properties

Specimen	Material (JIS)	Section (mm)	Sectional area (mm <sup>2</sup> )	Length			Slenderness ratio	$D/t$ $B/2t_f$	$\sigma_y$ (N/mm <sup>2</sup> )	$\sigma_u$ (N/mm <sup>2</sup> )	Elongation (%)
				$L_0$ (mm)	$L_B$ (mm)	$L_k$ (mm)					
P728	STK400	Dia89.1 × t3.2	864	2,456	2,127	1,617	70	28	365	456	27.1
H710	SS400	H-90 × 90 × t <sub>w</sub> 4.5 × t <sub>f</sub> 4.5	1,175	1,865	1,511	1,046	70	10	327	430	28.0



**Fig. 9.** Test loading protocol: (a) gradually increasing cyclic amplitude; (b) gradually decreasing cyclic amplitude; (c) eccentrically increasing cyclic amplitude; (d) random cyclic amplitude



**Fig. 10.** Experimentally determined force–deformation relationships of circular tube braces (P728): (a) gradually increasing; (b) gradually decreasing; (c) eccentrically increasing; (d) random

- Eccentrically increasing cyclic amplitude: As shown in Fig. 9(c), the tensile-normalized axial deformation was initially  $\varepsilon_n = 1.0\%$ ; the half-amplitudes of 0.1, 0.5, and 1.0% were then induced around the center of  $\varepsilon_n = 1.0\%$  for three cycles each followed by the final amplitude until brace fracture.
- Random cyclic amplitude: As shown in Fig. 9(d), random amplitudes of 0.1–1.0% were induced with normalized axial deformation. The process shown in Fig. 9(d) was defined as one set, and the same set was repeated until brace fracture.

Figs. 10(a–d) show the  $\varepsilon_n$ – $\sigma_n$  relationships obtained from the tests on the circular-tube braces, and Figs. 11(a–d) show those of the H-section braces. Table 2 lists the amplitudes and the numbers of cycles at which the braces experienced overall buckling, local buckling, cracking, and fracture. The circled numbers for random cyclic amplitude mean the step number indicated in the Fig. 9. With gradually increasing amplitudes, both braces experienced overall buckling during the first excursion to  $\varepsilon_n = 0.5\%$ . Local buckling occurred at  $\varepsilon_n = 1.0\%$  in the circular tube and

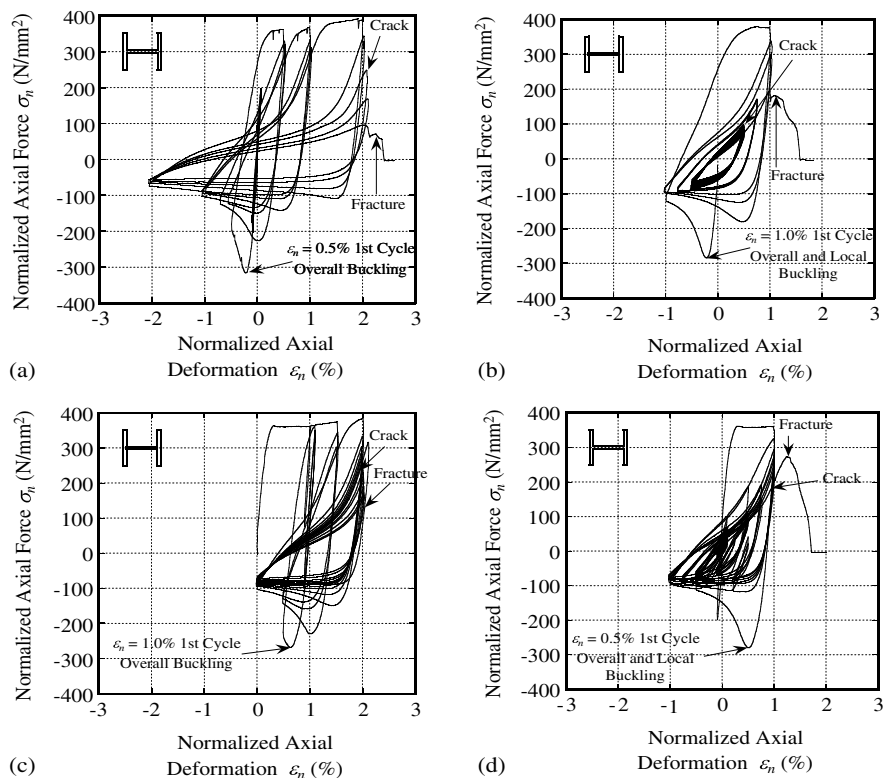


**Fig. 11.** Experimentally determined force–deformation relationships of circular tube braces (H710): (a) gradually increasing; (b) gradually decreasing; (c) eccentrically increasing; (d) random

**Table 2.** Results of Each Loading Test

Specimen	Loading history	Global buckling	Local buckling	Crack	Fracture
P728	Gradually increasing	1st cycle at 0.5%	1st cycle at 1.0%	1st cycle at 2.0%	1st cycle at 2.0%
	Gradually decreasing	1st cycle at 1.0%	1st cycle at 1.0%	2nd cycle at 0.75%	2nd cycle at 0.5%
	Eccentrically increasing	1st cycle at 0.5%	2nd cycle at 1.0%	5th cycle at 1.0%	5th cycle at 1.0%
	Random	cycle ③ in 1st set	cycle ③ in 1st set	cycle ② in 2nd set	cycle ② in 2nd set
H710	Gradually increasing	1st cycle at 0.5%	2nd cycle at 0.5%	3rd cycle at 2.0%	5th cycle at 2.0%
	Gradually decreasing	1st cycle at 1.0%	1st cycle at 1.0%	21th cycle at 0.5%	37th cycle at 0.5%
	Eccentrically increasing	1st cycle at 0.5%	2nd cycle at 0.5%	10th cycle at 1.0%	10th cycle at 1.0%
	Random	cycle ③ in 1st set	cycle ③ in 1st set	cycle ② in 3rd set	cycle ② in 3rd set

**Table 3.** Cumulative Normalized Deformation until Fracture (%)

Specimen	Loading history			
	Gradually increasing	Gradually decreasing	Eccentrically increasing	Random
P728	24.52	17.55	44.36	30.21
H710	42.22	62.57	66.63	64.6

$\epsilon_n = 0.5\%$  in the H-section. However, the H-section survived until the fifth cycle of  $\epsilon_n = 2.0\%$ , whereas the circular tube fractured at the first cycle of  $\epsilon_n = 2.0\%$ . Table 3 lists the values of cumulative normalized axial deformations until fracture. The circular tube brace fractured at the smallest value of cumulative deformation under the gradually decreasing loading history, whereas the H-section brace failed at the smallest cumulative deformation under the gradually increasing loading history. Fig. 12 shows the typical shape of local buckling and fracture in each specimen. All fractures initiated from the corner of the local buckling, as assumed in the previous section. It has been pointed out in past research that the

cumulative deformation capacities until fractures for open-section braces as H-braces are larger than those of closed sections as circular-hollow sections. The above results indicate that the H-section braces had greater cumulative normalized axial deformation values than the circular braces in all cases.

### FEM Analysis of Cyclic Loading Tests on Braces

The behaviors of the circular-tube and H-section braces after local buckling were simulated using *ABAQUS* (version 6.7-1), an FEM analysis software package, for determining the local strain distributions. Fig. 13 shows the analysis models. Each brace was composed of shell finite elements including connections. Each element contained four nodes and three shell layers with seven integral points in the thickness direction to evaluate the surface plastic strain at local buckling zones. Material characteristics were calibrated based on the results of tension coupon tests. An overall hardening rule involving isotropic and kinematic hardening was adopted. Fig. 14 shows that the analytically obtained  $\epsilon_n - \sigma_n$  hysteresis

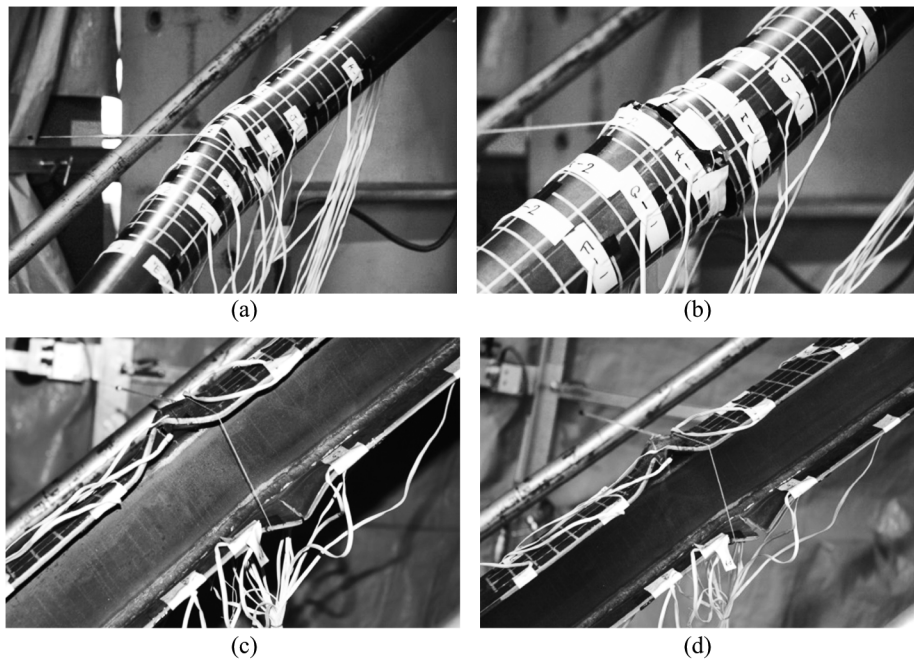


**Fig. 12.** Local buckling and fracture processes: (a) local buckling of circular tube brace; (b) fracture of circular tube brace; (c) local buckling of H-section brace; (d) flange fracture of H-section brace

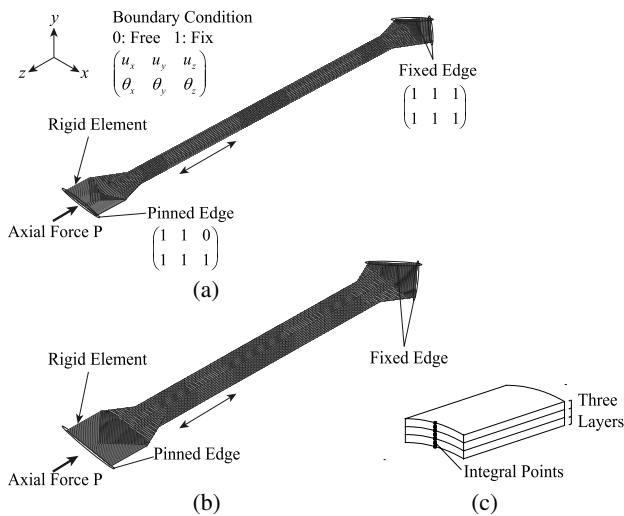


**Fig. 13.** FEM analysis models: (a) circular tubular brace; (b) H-section brace; (c) shell element

curves were nearly consistent with the experimental results. Fig. 15 shows the comparison of local plastic strain transitions at local buckling zones obtained from FEM analyses with measured strain near the local buckling zones in experiments, which shows the similar tendency. Plastic-strain transitions Fig. 16 show the local out-of-plane deflection and local strain distribution at the local buckling zone in each specimen together with the local deformation distribution at  $\epsilon_n = 2.0\text{--}3.0\%$ . In the figures, the local strain-distribution values calculated using Eqs. (1) and (13) are plotted as dotted lines. The local strain values predicted using the proposed equations generally agreed with the maximum values obtained from the FEM analysis, regardless of the loading history. The local strain-amplitude transitions along each loading history as obtained in the FEM analysis are shown in Fig. 18 using black circles, where Figs. 18(a–d) represent the circular tube braces and Figs. 18(e–h) represent the H-section braces. The local strain amplitudes assessed using Eqs. (1) and (13) are represented by solid lines in Fig. 17. In all specimens, the increases in the local strain amplitudes after the occurrence of local buckling according to the proposed formulas were generally consistent with the strain transitions obtained in the FEM analysis.

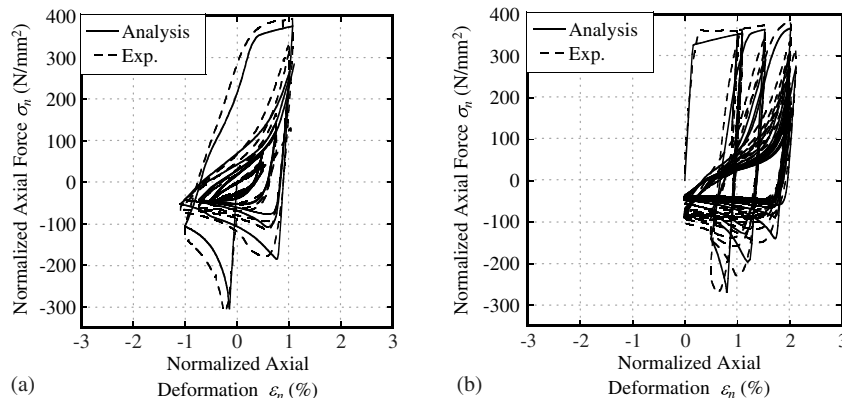


**Fig. 14.** Comparison of hysteresis between analyses and experiments: (a) gradually increasing (P728); (b) eccentrically increasing (H710)

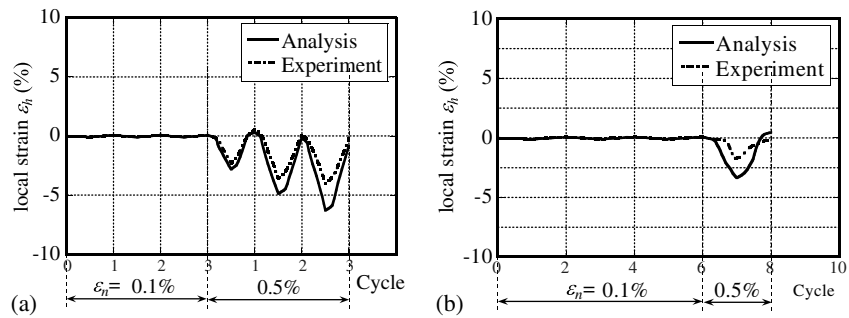


**Fig. 15.** Comparison of local strain between analyses and experiments: (a) gradually increasing (P728); (b) gradually increasing (H710)

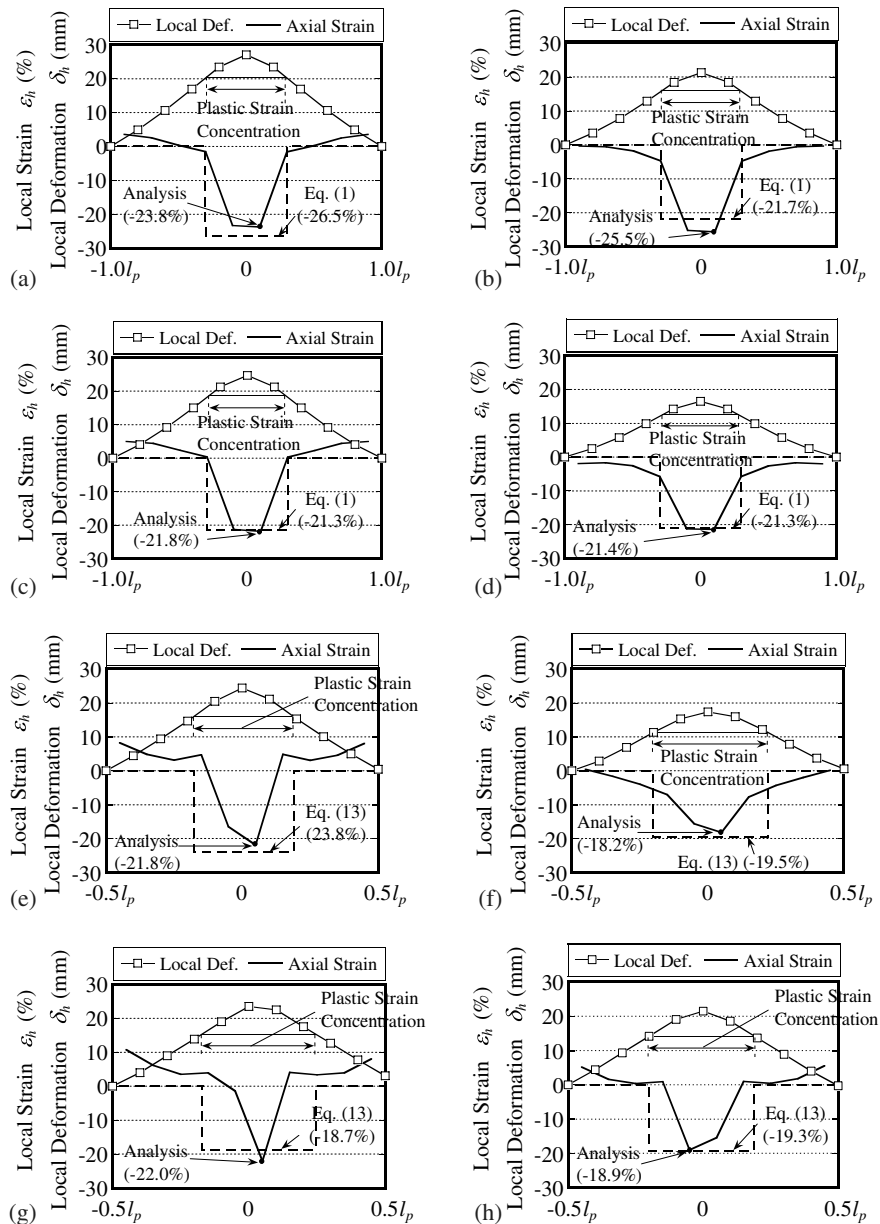


**Fig. 16.** Local stress and deformation at local buckling areas: (a) gradually increasing (P728); (b) gradually decreasing (P728); (c) eccentrically increasing (P728); (d) random (P728); (e) gradually increasing (H710); (f) gradually decreasing (H710); (g) eccentrically increasing (H710); (h) random (H710)

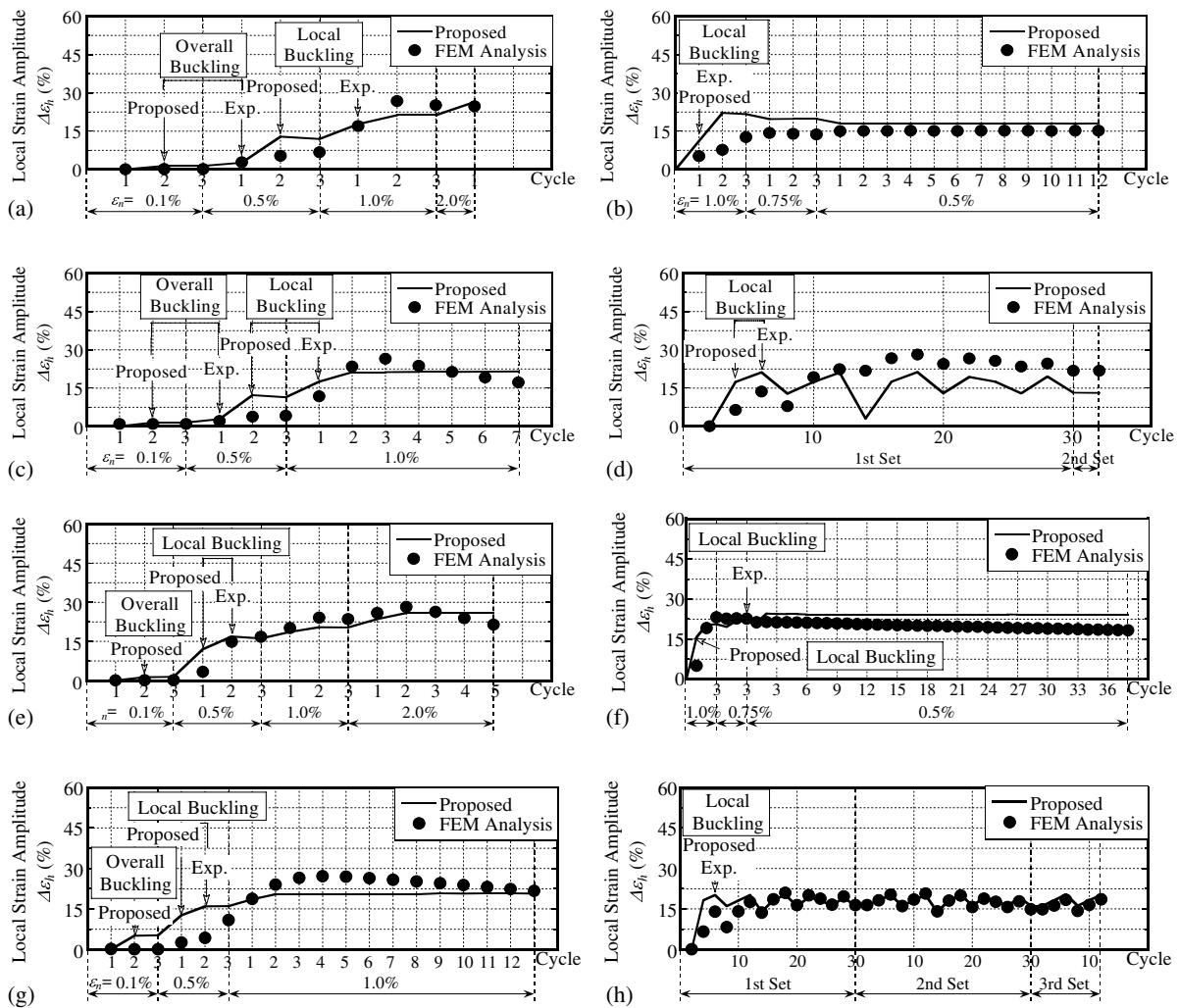


**Fig. 17.** Estimated local strain transitions: (a) gradually increasing (P728); (b) gradually decreasing (P728); (c) eccentrically increasing (P728); (d) random (P728); (e) gradually increasing (H710); (f) gradually decreasing (H710); (g) eccentrically increasing (H710); (h) random (H710)

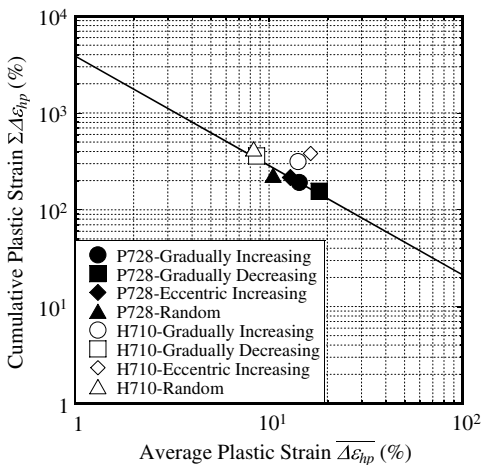


**Fig. 18.** Cumulative plastic strain at fracture

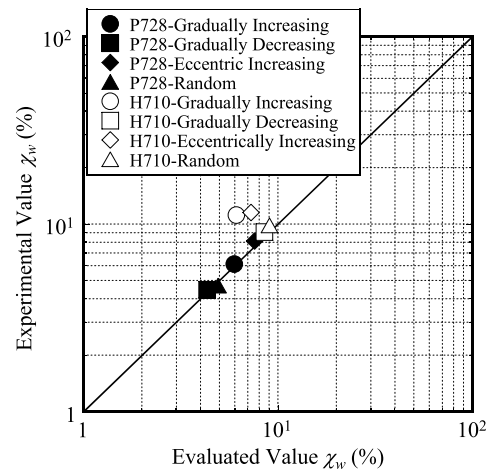


**Fig. 19.** Accuracy of proposed method

Fig. 18 plots the cumulative local plastic strain and the average plastic strain at the local buckling zone, which were calculated from the analyses until the instant of fracture in the experiment. The solid line denotes the low-cycle fatigue curve of the material [JIS SS400

(JIS 2010); Saeki et al. 1995], whose triaxial stress conditions are similar as the stress at local buckling zones, and the moment of fracture may be determined from the fatigue curves. This means that the braces fracture at the moment when the evaluated

cumulative local strain reaches the fatigue curves of the material. The moment of fracture is considered as the instant at which the cumulative local plastic strain, estimated as the product of the normalized axial deformation and the strain-concentration ratio obtained using the proposed formulas, reaches the low-cycle fatigue curve. Fig. 19 compares the normalized cumulative dissipation energy  $\chi = \sum \sigma_n(\Delta\varepsilon_n - 2\varepsilon_y)/\sigma_y$  until fracture obtained using the proposed method and with that obtained from the experimental results. Here,  $\sigma_y$  denotes yield stress. Although the proposed method showed the errors of twice smaller in maximum in some amplitudes for H-sections, all other results generally agreed well for all loading histories; therefore, the proposed method is considered to be valid for not only gradually increasing loading amplitudes but also for other types of amplitudes.

## Conclusion

A simple method for assessing the cumulative deformation capacities of circular-tube and H-section braces until fracture under cyclic loadings using physical macro models is proposed. A series of cyclic-loading tests was carried out on these braces under not only gradually increasing amplitudes but also various loading histories. The fracture mechanism was clarified by FEM analysis, and the strain-concentration ratios and cumulative deformation capacities until fracture assumed in the proposed formulas were compared with the experimental results. The obtained conclusions are summarized as follows:

1. Both braces underwent overall buckling at the half amplitudes of the normalized axial deformation of  $\varepsilon_n = 0.5\%$ , and local buckling occurred at  $\varepsilon_n = 1.0\%$  in the circular tube and  $\varepsilon_n = 0.5\%$  in the H-section. The H-section fractured during the fifth cycle of  $\varepsilon_n = 2.0\%$ , whereas the circular tube fractured during the first  $\varepsilon_n = 2.0\%$  cycle. Generally, the H-section braces survived longer than the circular-tube braces. Among all loading histories, the circular-tube brace fractured at the smallest values of cumulative deformation under the gradually decreasing loading history, whereas the H-section brace fractured at the smallest cumulative deformation under the gradually increasing loading history.
2. The FEM results indicated that plastic strain intensely increased in the strain-concentration region after local buckling, and the local strain reached 15–30%, thus leading to brace fracture.
3. The strain concentration ratio index was used for introducing a method to evaluate the cumulative deformation capacities of the circular-tube and H-section braces until fracture. The local strain amplitudes at the fracture point in FEM analyses were generally consistent with the values assumed by the proposed formulas for all types of loading histories.
4. The moment of fracture and the energy dissipated until fracture predicted by the proposed method agreed well with the test results for all types of loading histories, and the use of the proposed method for estimating the moment of fracture regardless of the loading pattern was validated.

With this methodology, brace fracture after buckling can be predicted easily using phenomenological macro model analyses, including postbuckling hysteresis. Post brace-fracture analysis of CBFs is also possible by eliminating the fractured braces in the time–history process. Post brace-fracture analyses of actual structures damaged by past earthquakes are being carried out, and the validity of the proposed fracture-evaluation method is being confirmed; this will be reported in future papers.

## Appendix. Postbuckling Hysteresis Model by Shibata–Wakabayashi

Detailed formulas of the Shibata–Wakabayashi model proposed by Shibata (1982), shown in Fig. 1, are described in the following. In the figure,  $\Delta$  denotes the normalized axial deformation ( $\varepsilon_n$  in the text),  $\Delta_y$  denotes the yield-normalized axial deformation ( $\varepsilon_y$  in the text),  $n$  denotes the normalized axial force by  $n_y$ , and  $n_y$  denotes the yield axial force. Point *A* is the tension yield critical point, *B* is the compression-buckling critical point, *P* is the partial tensile-yielding critical point, and *Q* is the release point following the buckling path. The normalized axial force,  $n$ , for the relevant stage is given by Eq. (15), and the related parameters in Eq. (15) are obtained using Eqs. (16)–(20). Furthermore, modification formulas expressing the degradation of buckling force under cyclic hysteresis are proposed and confirmed for accurately representing postbuckling behavior, including elasto-plastic buckling

$$n = \begin{cases} 1 & \text{[Stage A]} \\ f_i(\Delta_A - \Delta) & \text{[Stage B]} \\ -f_c(\Delta_B + n_c - \Delta) & \text{[Stage C]} \\ n_p + \frac{(\Delta - \Delta_p)(n_p - n_Q)}{\Delta_p - \Delta_Q} & \text{[Stage D]} \end{cases} \quad (15)$$

$$f_c(X) = (p_1X + p_2)^{-0.5} \quad (16)$$

$$f_i(X) = (p_3X + 1)^{-1.5} \quad (17)$$

$$p_1 = \left( \frac{10\lambda^2\sigma_y}{3\pi^2E} - \frac{1}{3} \right) \quad (18)$$

$$p_2 = \left( \frac{4\lambda^2\sigma_y}{\pi^2E} + 0.6 \right) \quad (19)$$

$$p_3 = 1 / \left( \frac{3.1\pi^2E}{\lambda^2\sigma_y} + 1.4 \right) \quad (20)$$

where  $\lambda_i$  = slenderness ratio of the brace; and  $n_c$  = solution of Eq. (21).

$$p_1n_c^3 + p_2n_c - 1 = 0 \quad (21)$$

In the case that the stage changes, the reference points *A*, *B*, *P*, and *Q* are defined with the following equations.

[Release in Stage A]

$$\begin{aligned} \Delta_{\text{new}}^A &= \Delta_{\text{old}}^P = \Delta & n_{\text{new}}^P &= 1 \\ \Delta_{\text{new}}^B &= \Delta_{\text{new}}^Q = \Delta - 1 - n_c & n_{\text{new}}^Q &= -n_c \end{aligned} \quad (22)$$

[Release in Stage B]

$$\begin{aligned} \Delta_{\text{new}}^B &= \Delta_{\text{old}}^B + (\Delta_{\text{old}}^A - 1 - n_c - \Delta_{\text{old}}^B) \frac{\Delta - \Delta_{\text{old}}^P}{\Delta_{\text{old}}^A - \Delta_{\text{old}}^P} \\ \Delta_{\text{new}}^P &= \Delta & n_{\text{new}}^P &= n & \Delta_{\text{new}}^Q &= \Delta_{\text{new}}^B - \frac{(\Delta_{\text{new}}^A - \Delta)}{q_3} \\ n_{\text{new}}^Q &= -f_c(\Delta_{\text{new}}^B + n_c - \Delta_{\text{new}}^Q) \end{aligned} \quad (23)$$

$$q_3 = 0.3\sqrt{n_E} + 0.24 \quad n_E = \frac{\pi^2 E}{\lambda^2 \sigma_y} \quad (\text{Euler buckling stress}) \quad (24)$$

[Release in Stage C]

$$\begin{aligned} \Delta_{\text{new}}^A &= \Delta_{\text{old}}^A + \ln[q_1(\Delta_{\text{old}}^Q - \Delta) + 1] - q_2(\Delta_{\text{old}}^B - \Delta_{\text{old}}^Q) \geq \Delta_{\text{old}}^A \\ \Delta_{\text{new}}^Q &= \Delta \quad n_{\text{new}}^Q = n \quad \Delta_{\text{new}}^P = \Delta_{\text{new}}^A - q_3(\Delta_{\text{old}}^B - \Delta) \\ n_{\text{new}}^P &= f_t(\Delta_{\text{new}}^A - \Delta_{\text{new}}^P) \end{aligned} \quad (25)$$

$$q_1 = \left(3 - \frac{1}{n_E}\right) / 10 \quad q_2 = \frac{0.115}{n_E} + 0.36 \quad (26)$$

## Notation

The following symbols are used in this paper:

- $A$  = original sectional area;
- $B$  = width of H-section;
- $D$  = circular tube diameter;
- $E$  = elastic modulus of steel;
- $L_B$  = distance between plastic hinges on both gusset plates;
- $L_k$  = effective plastic buckling length of brace;
- $L_h$  = plastic hinge zone length;
- $l_p$  = local buckling wavelength;
- $l_{pk}$  = effective plastic local buckling wavelength;
- $M_{pb}$  = yield bending moment of brace;
- $M_{pg}$  = yield bending moment of gusset plate;
- $N_f$  = number of cycles to steel fracture;
- $P$  = axial force on brace;
- $S$  = section modulus of brace (weak axis of H-section);
- $S_l$  = section modulus of local buckling zone;
- $t_f$  = thickness of circular tube or H-section flange;
- $Z$  = plastic section modulus of brace (weak axis of H-section);
- $Z_l$  = plastic section modulus of local buckling zone;
- $\alpha_c$  = strain concentration ratio;
- $\Delta\varepsilon_h$  = local strain amplitude in hinge zone strain;
- $\Delta\varepsilon_n$  = normalized axial deformation amplitude;
- $\Delta\theta_h$  = incremental angle of hinge zone that influences local buckling;
- $\overline{\Delta\varepsilon}_{hp}$  = average plastic strain amplitude in hinge zone;
- $\Delta$  = axial displacement of brace;
- $\varepsilon_{cr}$  = overall buckling strain ( $\sigma_{cr}/E$ );
- $\varepsilon_n$  = normalized axial deformation;
- $\varepsilon_{ntm}$  = maximum tensile-normalized axial deformation;
- $\varepsilon_h$  = local strain in hinge zone;
- $\varepsilon_{hp}$  = local plastic strain in hinge zone;
- $\varepsilon_{lb}$  = equivalent strain attain to local buckling;
- $\varepsilon_y$  = yield strain;
- $\theta_h$  = angle of hinge zone;
- $\theta_{lb}$  = angle of plastic hinge due to local buckling;
- $\sum \Delta\varepsilon_{hp}$  = cumulative plastic strain in hinge zone;
- $\sigma_{cr}$  = overall buckling stress;
- $\sigma_n$  = normalized stress;

- $\sigma_y$  = yield stress;
- $\phi$  = vertical angle of local buckling wave (H-section); and
- $\varphi_h$  = angle of skin plate at local buckling zone.

## References

- Elchalakani, M., Zhao, X.-L., and Grzebieta, R. (2003). "Tests on cold-formed circular tubular braces under cyclic axial loading." *J. Struct. Div.*, 10.1061/(ASCE)0733-9445(2003)129:4(507), 507–514.
- Fell, B. V., Kanvinde, A. M., Deierlein, G. G., and Myers, A. T. (2009). "Experimental investigation of inelastic cyclic buckling and fracture of steel braces." *J. Struct. Eng.*, 10.1061/(ASCE)0733-9445(2009)135:1(19), 19–32.
- Hsiao, P. C., Lehman, D. E., and Roeder, C. W. (2013). "A model to simulate special concentrically braced frames beyond brace fracture." *Earthquake Eng. Struct. Dyn.*, 42(2), 183–200.
- Jain, A. K., Goel, S. C., and Hanson, R. D. (1978). "Inelastic response of restrained steel tubes." *J. Struct. Div.*, 104(6), 897–910.
- Jain, A. K., Goel, S. C., and Hanson, R. D. (1980). "Hysteresis cycles of axially loaded steel members." *J. Struct. Div.*, 106(8), 1777–1795.
- Japanese Industrial Standard (JIS). (2010). "JIS G 3101: Rolled steels for general structure." *SS400*.
- Kanvinde, A. M., and Deierlein, G. G. (2007). "Finite element simulation of ductile fracture in reduced section pull plates using micromechanics-based fracture models." *J. Struct. Eng.*, 10.1061/(ASCE)0733-9445(2007)133:5(656), 656–664.
- Kato, B., and Nakao, M. (1994). "Strength and deformation capacity of H-shaped steel members governed by local buckling." *J. Struct. Constr. Eng. Trans. AIJ*, 458(4), 127–136.
- Li, G., Fahnestock, L. A., and Li, H. (2013). "Simulation of steel brace hysteretic response using the force analogy method." *J. Struct. Eng.*, 10.1061/(ASCE)ST.1943-541X.0000664, 526–536.
- Popov, E. P., Zayas, V. A., and Mahin, S. A. (1979). "Cyclic inelastic buckling of thin tubular columns." *J. Struct. Div.*, 105(11), 2261–2277.
- Prathuangsit, D., Goel, S. C., and Hanson, R. D. (1978). "Axial hysteresis behavior with end restraints." *J. Struct. Div.*, 104(6), 883–896.
- Saeki, E., Sugisawa, M., Yamaguchi, T., Mochizuki, H., and Wada, A. (1995). "A study on low cycle fatigue characteristics of low yield strength steel." *J. Struct. Constr. Eng. Trans. AIJ*, 472(6), 139–147.
- Shibata, M. (1982). "Analysis of elastic-plastic behavior of a steel brace subjected to repeated axial force." *Int. J. Solid Struct.*, 18(3), 217–228.
- Takeuchi, T., and Matsui, R. (2011). "Cumulative cyclic deformation capacity of circular tubular braces under local buckling." *J. Struct. Eng.*, 10.1061/(ASCE)ST.1943-541X.0000380, 1311–1318.
- Takeuchi, T., Qin, K., and Matsui, R. (2008). "Cumulative cyclic deformation capacity of H-section braces with local buckling." *J. Struct. Constr. Eng., Trans. AIJ*, 73(632), 1875–1882.
- Tang, X., and Goel, S. C. (1989). "Brace fractures and analysis of phase I structure." *J. Struct. Div.*, 10.1061/(ASCE)0733-9445(1989)115:8(1960), 1960–1976.
- Timoshenko, S., and Gere, J. (1961). *Theory of elastic stability*, McGraw-Hill.
- Tremblay, R. (2002). "Inelastic seismic response of steel bracing members." *J. Constr. Steel Res.*, 58(5–8), 665–701.
- Tremblay, R. (2008). "Influence of brace slenderness on the fracture life of rectangular tubular steel bracing members subjected to seismic inelastic loading." *ASCE Structural Congress*, ASCE-SEL, VA.
- Uriz, P., Mahin, S. A. (2004). "Seismic vulnerability assessment of concentrically braced steel frames." *Steel Struct.*, 4(4), 239–248.